# Stable propagation of mechanical signals in soft media using stored elastic energy

Jordan R. Raney[a,b], Neel Nadkarni[c], Chiara Daraio[d,e], Dennis M. Kochmann[c,1], Jennifer A. Lewis[a,b,1], and Katia Bertoldi[a,f,1]

[a]John A. Paulson School of Engineering and Applied Sciences, Harvard University, Cambridge, MA 02138; [b]Wyss Institute for Biologically Inspired Engineering, Harvard University, Cambridge, MA 02138; [c]Graduate Aerospace Laboratories, California Institute of Technology, Pasadena, CA 91125; [d]Engineering and Applied Science, California Institute of Technology, Pasadena, CA 91125; [e]Department of Mechanical and Process Engineering, ETH Zurich, 8092 Zurich, Switzerland; and [f]Kavli Institute, Harvard University, Cambridge, MA 02138

Edited by Monica Olvera de la Cruz, Northwestern University, Evanston, IL, and approved June 27, 2016 (received for review March 24, 2016)

**Soft structures with rationally designed architectures capable of large, nonlinear deformation present opportunities for unprecedented, highly tunable devices and machines. However, the highly dissipative nature of soft materials intrinsically limits or prevents certain functions, such as the propagation of mechanical signals. Here we present an architected soft system composed of elastomeric bistable beam elements connected by elastomeric linear springs. The dissipative nature of the polymer readily damps linear waves, preventing propagation of any mechanical signal beyond a short distance, as expected. However, the unique architecture of the system enables propagation of stable, nonlinear solitary transition waves with constant, controllable velocity and pulse geometry over arbitrary distances. Because the high damping of the material removes all other linear, small-amplitude excitations, the desired pulse propagates with high fidelity and controllability. This phenomenon can be used to control signals, as demonstrated by the design of soft mechanical diodes and logic gates.**

soft | mechanical signal | stable propagation | instability

Soft, highly deformable materials have enabled the design of new classes of tunable and responsive systems and devices, including bioinspired soft robots (1, 2), self-regulating microfluidics (3), adaptive optics (4), reusable energy-absorbing systems (5, 6), structures with highly programmable responses (7), and morphological computing paradigms (8). However, their highly deformable and dissipative nature also poses unique challenges. Although it has been demonstrated that the nonlinear response of soft structures can be exploited to design machines capable of performing surprisingly sophisticated functions on actuation (1, 2, 9), their high intrinsic dissipation has prevented the design of completely soft machines. Sensing and control functionalities, which require transmission of a signal over a distance, still typically rely on the integration of stiff electronic components within the soft material (10, 11), introducing interfaces that are often a source of mechanical failure.

The design of soft control and sensing systems (and, consequently, completely soft machines) requires the ability to propagate a stable signal without distortion through soft media. There are two limiting factors intrinsic to materials that work against this: dispersion (signal distortion due to frequency-dependent phase velocity) and dissipation (loss of energy over time as the wave propagates through the medium). Dispersion can be controlled or eliminated through nonlinear effects produced via the control of structure in the medium (12). For example, periodic systems based on Hertzian contact (13–15), tensegrity structures (16), rigid bars and linkages (17), and bistable elastic elements (18) can behave as nondispersive media, with the nonlinearity of their local mechanical response canceling out the tendency for the signal to disperse at sufficiently large amplitudes. However, dissipation is still an overarching problem. Structures designed to propagate elastic waves are typically built from stiff materials with low intrinsic dissipation (e.g., metals) and excited with small-amplitude excitation (to avoid plastic energy loss). This approach minimizes, but does not eliminate, dissipation. In soft, highly dissipative media, the problem is further exacerbated, and there is no robust strategy currently available to propagate signals in these systems.

Here we report an architected medium made of a highly dissipative, soft material that overcomes both dispersive and dissipative effects and enables the propagation of a mechanical signal over arbitrary distances without distortion. A stable mechanical signal can be transmitted over long distances through a dissipative medium only if additional energy is continuously supplied during its propagation. To achieve such behavior, we use bistable elastomeric beams that are capable of storing elastic energy in the form of deformation and then, stimulated by the wavefront, releasing it during the propagation of the wave, without the need of any external stimulus. Dissipation allows stable wave propagation by balancing the elastic energy release. The damping intrinsic to the soft materials removes all signals except the desired transition wave, which therefore propagates with high fidelity, predictability, and controllability. Furthermore, as observed for nondissipative (18) or minimally dissipative systems (19) made from stiff materials, a series of interacting bistable units can transmit nondispersive transition waves. By contrast, the proposed architecture is capable of propagating stable waves with constant velocity over arbitrary distances, overcoming both dissipative and dispersive effects, despite the soft, dissipative material of which it is composed. Together, these effects enable the design of functional devices such as soft mechanical logic elements. The ability to 3D print soft mechanical logic enables a higher degree of customizability and tunability relative to previous examples of mechanical logic (15, 20–22).

## Significance

**Advances in nonlinear mechanics have enabled the realization of a variety of nontraditional functions in mechanical systems. Intrinsic dissipation typically limits the utility of these effects, with soft polymeric materials in particular being incompatible with meaningful wave propagation. Here we demonstrate a nonlinear soft system that is able to propagate large-amplitude signals over arbitrary distances without any signal degradation. We make use of bistable beams to store and then release elastic energy along the path of the wave, balancing both dissipative and dispersive effects. The soft and 3D printable system is highly customizable and tunable, enabling the design of mechanical logic that is relevant to soft autonomous systems (e.g., soft robotics).**

Author contributions: J.R.R., C.D., D.M.K., J.A.L., and K.B. designed research; J.R.R. and N.N. performed research; J.R.R. contributed new reagents/analytic tools; J.R.R., N.N., C.D., D.M.K., J.A.L., and K.B. analyzed data; and J.R.R., N.N., C.D., D.M.K., J.A.L., and K.B. wrote the paper.

The authors declare no conflict of interest.

This article is a PNAS Direct Submission.

[1]To whom correspondence may be addressed. Email: bertoldi@seas.harvard.edu, kochmann@caltech.edu, or jalewis@seas.harvard.edu.

This article contains supporting information online at www.pnas.org/lookup/suppl/doi:10.1073/pnas.1604838113/-/DCSupplemental.

## System Architecture

The fundamental building block of our system is a bistable element (formed by two tilted beams) connected to a horizontal element with linear response, all made of elastomeric material (Fig. 1*A*). The tilted beams have aspect ratio $L/t = 18$ (with $L = 7$ mm), whereas their inclination angle is determined by their end-to-end distance $d$. The horizontal coupling elements are designed to have a linear mechanical response (Fig. 1*B*), with their morphology selected to achieve a range of effective stiffnesses (an important parameter for determining the dynamic behavior of the system, as described later and shown in Fig. S1). Systems comprising up to 100 building blocks arranged to form a one-dimensional chain (Fig. 1*A*) are fabricated with high fidelity using direct ink writing, an extrusion-based 3D printing method (23). In this approach, viscoelastic inks are extruded through a fine deposition nozzle that undergoes programmed translation to create 3D structures layer by layer (24–26). Direct ink writing is particularly well suited for producing our structures because narrow features with tunable aspect ratios can be readily fabricated by locally varying the print velocity. Here we used a polydimethylsiloxane (PDMS) ink and followed the processing steps outlined in *Materials and Methods*. After printing, a stiff support structure is infilled adjacent to the soft architecture to ensure uniform morphology of the soft elements along the length of the system and to enable precise control of the end-to-end distance $d$, which defines the beam orientation and the resulting mechanical response of the bistable elements.

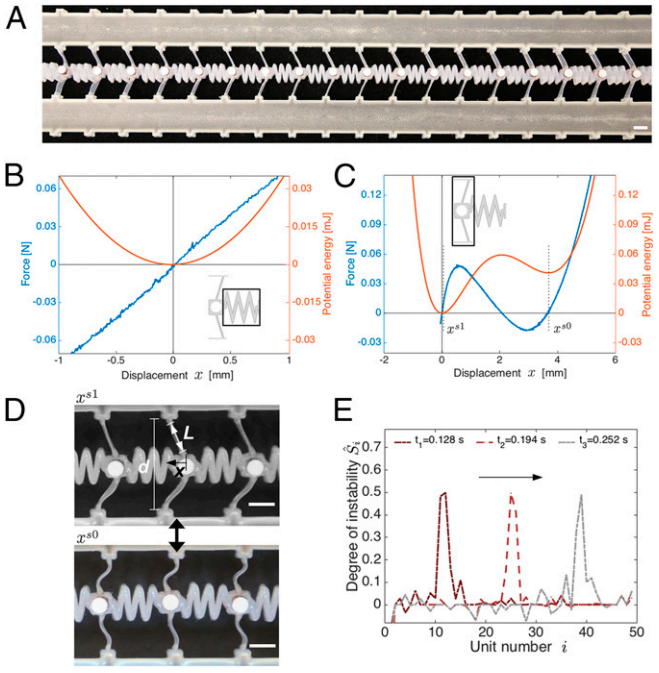


**Fig. 1.** (*A*) The system consists of a 1D series of bistable elements connected by soft coupling elements. (Scale bar, 5 mm.) (*B*) The coupling elements are designed to exhibit a linear mechanical response, whereas (*C* and *D*) the bistable elements possess two stable states. The bistability originates from lateral constraint ($d$) on a beam pair that is displaced ($x$) perpendicularly to the constraint. The mechanical response is fully determined by the aspect ratio ($L$ divided by the thickness of the beam) and $d$. The two stable configurations of the bistable element correspond to the displacements $x = x^{s1} = 0$ and $x = x^{s0}$. (Scale bars, 5 mm.) (*E*) In certain cases a stable nonlinear transition wave propagates through the system (with each bistable element undergoing a displacement from $x = x^{s0}$ to $x = x^{s1}$). The instability ($\hat{S}_i$) propagates with constant velocity and geometry, enabled by both (*i*) the balance of nonlinear and dispersive effects and (*ii*) the balance of dissipation and energy release. Here we show snapshots of the evolving state of the chain, with $t_1 = 0.128$ s, $t_2 = 0.194$ s, and $t_3 = 0.252$ s relative to the start of the experiment, in this case with $d = 18.6$ mm.

Additionally, a small copper cylinder is press fit in the middle of each bistable element, which serves both to add a concentrated mass at each node and to provide contrast for optically tracking the wave propagation during subsequent experiments.

We start by characterizing the static response of both the bistable elements and the connecting horizontal elements. The force–displacement curve in Fig. 1*B* shows the linear response of the horizontal elements. In particular, for the element shown in Fig. 1*A*, with a zigzag morphology of length 10 mm, width 5 mm, and thickness 5.4 mm, we measure a stiffness $k = dF/dx = 80$ N/m. Note that the value of $k$ can be significantly altered by choosing different connector geometries or different extrusion rates during printing (Fig. S1). In contrast with the linear response of the connecting elements, the bistable elements, each composed of two tilted beams, are characterized by a highly nonlinear response with a regime of negative incremental stiffness (see the region with negative slope in Fig. 1*C*). The associated instability leads to a rapid shape change that has been studied in the context of both natural (27) and synthetic systems (28–31). The associated potential energy, $V(x)$ (defined such that $\partial V/\partial x = -F$ and calculated by first fitting a fifth-degree polynomial to the measured force–displacement data and then integrating), is characterized by two local minima at $x = x^{s1} = 0$ and $x = x^{s0}$ (Fig. 1*C*), corresponding to the two stable states shown in Fig. 1*D*. The stable configuration at $x^{s0}$ is characterized by an energy state higher than that of the undeformed one (at $x^{s1} = 0$). Therefore, similar to a phase transition, the transition between the two stable states involves a net change in stored potential energy, which, depending on the direction of the transition, either absorbs energy (5) or releases stored potential energy. In this work, we demonstrate that the release of energy associated with this transition can be exploited to overcome dissipation and to propagate a mechanical signal over arbitrary distances, enabling the design of soft and highly tunable devices, such as the mechanical logic elements demonstrated later.

## Response Under Large-Amplitude Excitations

Although the architected medium does not enable propagation of small-amplitude elastic waves over long distances due to the intrinsic damping of the polymer (Fig. S2), moderate- and large-amplitude excitation can lead to a very different response. If the bistable elements are initially set to their lower-energy (undeformed) stable configuration ($x = x^{s1} = 0$ in Fig. 1*C*, corresponding to the top image in Fig. 1*D*), displacing an element even to large amplitudes does not lead to a transition wave due to the energetically unfavorable (energy-absorbing) transition of each element (19). Therefore, because small-amplitude linear modes also disintegrate because of dissipation (Fig. S2), there exist no stable modes of energy transport when the elements are in the low-energy state. However, if the bistable elements are initially set to their higher-energy (deformed) stable configuration ($x = x^{s0}$ in Fig. 1*C*, corresponding to the bottom image in Fig. 1*D*), a sufficiently large displacement applied to any of the bistable elements can cause the displaced element to transition states, producing a nonlinear transition wave that propagates indefinitely outward from the point of initiation with constant speed and shape. This is due to both (*i*) an equilibrium between dispersive and nonlinear effects of the periodic structure (18) and (*ii*) a release of energy that equals the effects of dissipation as, stimulated by the wavefront, each of the bistable elements along the chain transitions from its higher- to lower-stable energy state (i.e., from $x = x^{s0}$ to $x = x^{s1} = 0$).

## Experimental Results

To characterize the propagation of such nonlinear waves experimentally, we used a high-speed camera and tracked the location of each bistable element along the chain as a function of time (Movie S1). Because at the wavefront the bistable elements transition from one stable configuration to the other, we monitor the displacement of each unit relative to its two stable configurations ($x^{s0}$ and $x^{s1}$). For the $i$th unit we therefore introduce two normalized distances

$$\hat{x}_i^{s1} = \left|\frac{x_i - x^{s1}}{x^{s0} - x^{s1}}\right|, \qquad \hat{x}_i^{s0} = \left|\frac{x^{s0} - x_i}{x^{s0} - x^{s1}}\right|, \qquad [1]$$

$x_i$ being the position of the $i$th bistable element along the chain. In Fig. 1*E* we visualize the propagation of the nonlinear wave by showing for each unit its normalized distance from the nearest stable configuration

$$\hat{S}_i = \min\left(\hat{x}_i^{s1}, \hat{x}_i^{s0}\right), \qquad [2]$$

at different times. If $\hat{S}_i = 0$, the $i$th element is in either of its two stable configurations, whereas $\hat{S}_i > 0$ indicates that the unit is passing through the energy barrier separating them. The experimental data of Fig. 1*E* clearly show that at the wavefront, a few bistable units (in this case, about four) are undergoing a change from one stable state to the other at any given time and that the transition sequentially propagates through the elements along the chain (Movie S2). We also find that this transition wave propagates with a constant shape, clearly indicating that both dispersive and dissipative effects are overcome in the structure.

The speed of the nonlinear wave can be obtained by monitoring the evolution of the normalized distance $\hat{x}^{s0}$ for each bistable unit during the entire experiment, as in Fig. 2*A*. Because in this contour map the blue and red colors indicate bistable units in the high-energy and low-energy stable configurations, respectively, the sequential change of each of the elements along the chain from one stable state to the other is evident. Furthermore, the constant slope of the boundary between the pretransition (blue) and posttransition (red) regions reveals a constant propagation velocity (in this case, $3.4 \pm 0.1$ m/s). Note also that the pulse width for any time can be extracted from the map by taking a horizontal slice of the plot (i.e., a fixed time) and measuring the number of bistable elements in the midst of transitioning between solid blue and solid red (approximately four elements in width).

Another unique aspect of this system is that the propagation velocity and pulse shape are the same (within the margin of error) whether the wave is initiated in compression or tension, as revealed by comparison of the contour plots reported in Fig. 2*A* (for compression) and Fig. 2*B* (for tension). In both cases, the transition wave propagates with a constant velocity (3.4 m/s) and pulse width (approximately four elements). The propagation of rarefaction pulses is a rare find and thus a noteworthy feature of this system. Although compressive nonlinear solitary waves have been observed in nonlinear periodic systems as in, e.g., Hertzian contact-based chains (12, 32, 33) as well as in macroscopic nonlinear chains using magnetic connectors (19, 34), rarefaction pulses have not been found in those, due to the lack of stiffness in tension, among other reasons. Finally, we note that the transition wave can also be initiated at any intermediate location along the chain, in which case a compressive pulse travels in one direction and a rarefaction pulse travels in the other direction, both propagating outward from the point of initiation (Movie S3).

## Numerical Results

We additionally characterized the transition wave propagation using a 1D mechanical model, in which the position $x_i(t)$ of the middle of the $i$th bistable element is governed by

$$m\frac{d^2x_i}{dt^2} - k[x_{i+1} - 2x_i + x_{i-1}] + \gamma\frac{dx_i}{dt} + \frac{dV}{dx_i} = 0, \qquad [3]$$

where $V$ is the quasi-1D on-site potential of each bistable element, $\gamma$ is a linear damping parameter, and $k$ is the connector spring stiffness. For a detailed discussion of the continuum limit and the energetic requirements for stable wave propagation, see ref. 35. The linear damping model is a leading-order approximation to the complex dissipative nature of elastomers. The bistable potential $V$ is numerically computed by nonlinear finite-element simulations of a quasistatically deforming, corotational, linear elastic beam in 2D (36). We validated the numerical force–displacement curves by comparison with the experimental data shown in Fig. 1*C* (see Fig. S3 for a comparison). To simulate the response of the system under large-amplitude excitations, initially, all nodes are placed in the high-energy configuration. The first node is then excited by displacing it from the high-energy stable point to the low-energy one, and the system response in time is solved using a Newmark-β scheme. The only unknown model parameter, $\gamma$, was determined by fitting experimental wave speed data for a particular combination of geometric parameters ($k = 80$ N/m and $d = 17.5$ mm, as defined in Fig. 1*D*; see Fig. S4 for the comparison between experiment and simulation). With all model parameters thereby determined, we examined systems with different combinations of geometric parameters. As an example, Fig. 2 *E* and *F* show simulated compression-initiated and tension-initiated pulses, respectively, which show excellent agreement with the experimental data discussed earlier (Fig. 2 *A* and *B*).

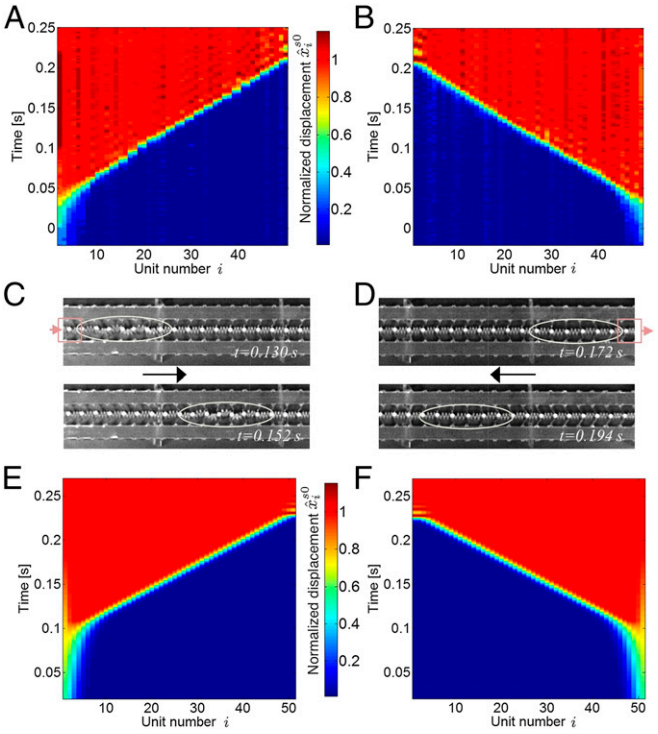


**Fig. 2.** The transition wave can be initiated anywhere along the chain, with compressive and rarefaction pulses proceeding in opposite directions from the point of initiation (here $d = 18.6$ mm). (*A* and *B*) The normalized displacements of the individual bistable elements ($\hat{x}_i$ for each of the $i$ elements in the chain) during the propagation of the wave, as recorded with a high-speed camera at 500 Hz. These panels show the propagation of the transition with a constant velocity and pulse width, after a brief initiation period during which steady-state is established. (*C* and *D*) Optical images of the experiments during wave propagation (obtained from a high-speed camera), corresponding to the data in *A* and *B*. (*E* and *F*) Simulations corresponding to the experiments shown in *A* and *B*, showing excellent quantitative agreement. For the compression-initiated pulse, the initiating displacement of the wave takes place on the left of the chain and is in the same direction as the pulse propagation; for the tension-initiated pulse, the initiating displacement takes place on the right of the chain, and the local tensile displacement is in the opposite direction of the wave propagation.

## Control of Wave Propagation

The results reported so far were obtained for a system with connecting elements of stiffness $k = 80$ N/m and bistable beams with aspect ratio $L/t = 18$ and constant end-to-end distance $d$. However,

both the width of the pulse and its propagation velocity can be greatly changed by manipulating either the nonlinear response of the bistable elements or the stiffness $k$ of the linear coupling elements. Although changes in $k$ require fabrication of new units with different morphology (Fig. S1), we can take advantage of the high deformability of soft materials to tune the nonlinear response of the bistable beams by applying small lateral loads to change the beam end-to-end distance $d$. With the demonstrated excellent quantitative agreement between numerical and experimental results, we used our simulations to systematically investigate the effects of the parameters $d$ and $k$ on the behavior of the propagating wave. First, the bistable on-site potential for different $d$ values was determined by analogous quasistatic 1D displacement-controlled simulations of an individual bistable element. The force–displacement curves obtained in this way were subsequently integrated to determine the on-site potential, and an eighth-order polynomial fit was used as an approximation for $V(x)$. The results reported in Fig. 3*A* for four representative values of $d$ show two key features. First, $d$ has a large effect on the energy barrier separating the two stable configurations, which is reflected also in changes in the peak forces during transition. Second, $d$ strongly affects the displacement necessary to obtain snap-through (from the high-energy state back to the low-energy state) and thereby to initiate the transition during wave propagation. Experiments were performed in which defined displacements were applied quasistatically to a bistable element for different values of $d$ (Fig. S5), confirming these trends.

Using these values for the on-site potential $V(x)$, simulations were subsequently performed to predict the wave characteristics for different connector element stiffnesses, $k$, and end-to-end distances, $d$. The wave speed (which is computed by tracking the point of maximum particle velocity) increases monotonically with increasing $k$ (Fig. 3*B*). However, the effect of $d$ on the wave velocity is more complicated. The wave velocity is highly sensitive to changes in $d$ when $d$ is small but much less sensitive when $d$ is large. The associated width of the transition wave was also noted, defined as the number of nodes that simultaneously have displacements between 10% and 90% of the transition displacement. The results reported in Fig. 3*C* indicate that the pulse width increases with increasing $k$, showing the same trend as the velocity. For a constant connector stiffness value $k$, $d$ does not have an effect on the width for lower stiffnesses but shows a similar variation as the velocity for higher stiffnesses. Experimental measurements of systems with different values of $d$ and $k$ (Figs. S6–S8) match these numerical results (Fig. 3) with excellent quantitative agreement, confirming the validity of our simulations.

The trends for velocity (Fig. 3*B*) and width (Fig. 3*C*) contours show a correlation with the energy barrier for different $d$ values as shown in Fig. 3*A*. For a constant interconnecting element stiffness, the $d$ values corresponding to high-energy barriers show lower velocity and width. This is because when the energy barrier is high, each element needs to absorb more energy to overcome the barrier, thereby causing a slower transition rate and therefore a lower wave speed and vice versa. Consequently, the energy barrier is the most important criterion in determining the transition speed and width of the displacement profile.

Because the $N$ bistable elements that constitute a particular pulse are not simultaneously in morphologies that place them in the peak of their individual energy barriers, the total pulse energy barrier, $E_{\text{tot}}$, is calculated as

$$E_{\text{tot}} = \sum_{j=1}^{N} V(x_j) - V(x^{s0}), \qquad [4]$$

where $V$ and $N$ are determined from the simulation results (Fig. 3 *A* and *C*, respectively) and the $x_j$ values are approximated by distributing them equally between $x^{s1}$ and $x^{s0}$ (i.e., $x_j = j\frac{x^{s0}-x^{s1}}{N+1}$). Fig. 3*D* shows this total potential energy barrier ($E_{\text{tot}}$), associated with the transition events of the individual bistable elements from their higher-energy state ($x = x^{s0}$) to their lower-energy state ($x = x^{s1}$). As expected, as the number of elements in the pulse ($N$) and the energy barrier for the individual elements increase, so does the total energy barrier required to initiate the pulse along a given portion of the chain because the total energy barrier is the sum of the transient barriers of the individual elements undergoing transition at a given time.

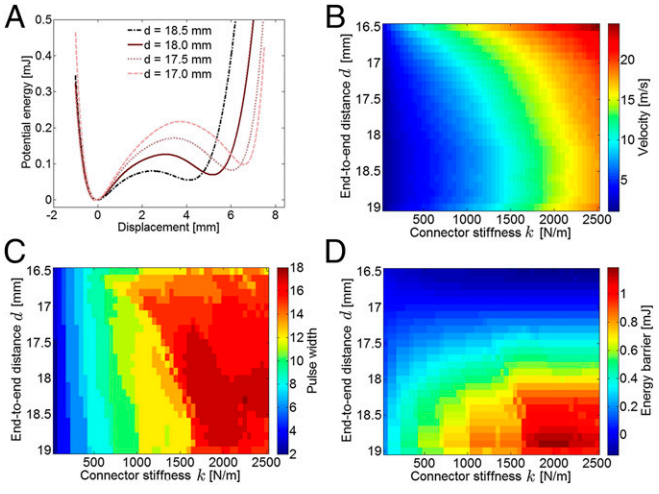


**Fig. 3.** (*A*) The on-site potential as a function of $x$ and $d$, as determined via quasistatic 1D displacement-controlled simulations of an individual bistable element. Simulated values of (*B*) pulse velocity and (*C*) pulse width as a function of end-to-end distance $d$ and connector stiffness $k$. (*D*) The measured energy landscape (*A*) of the individual bistable elements is combined with the simulated pulse widths (*C*) to compute an approximate energy barrier $E_{\text{tot}}$ for the entire propagating pulse (a function of both $d$ and $k$).

## Tunable Functional Devices

Having demonstrated that the energy barrier for a transition wave to propagate can be controlled by tuning $d$ and $k$, we now demonstrate how functional devices can be designed by carefully arranging the linear and nonlinear elements along the chain. To this end, it is critical to note that the pulse propagates independent of its initial conditions, so that it can be manipulated through entirely local geometric changes. This can be understood as a result of the high damping of the system, in which only the specific signal compatible with the local geometric parameters is able to propagate an appreciable distance.

For example, an accelerator can be designed by applying different values of $d$ spatially along the length of the system to achieve a controlled variation in velocity. This can be done without fabricating a specifically graded system because the deformable architecture allows different values of $d$ to be applied along the length of the system. The experimental results reported in Fig. S7 for a chain where $d$ is ∼14.5 mm at one end and about 19 mm at the other show an evident change in slope of the interface between the pretransitioned and posttransitioned states (blue and red, respectively), indicating a variation in pulse velocity (the slope of the interface is inversely proportional to the speed). In particular, we observe a change in the wave speed by more than a factor of 6 from the left end of the chain to the right (0.8–5.2 m/s). The velocity can be seen to continually vary along the length of the chain, but at each location it matches the expected velocities from Fig. 3*B*.

Further, a mechanical diode can be designed as a heterogeneous chain with soft linear horizontal connecting elements (corresponding to a low-energy barrier) in one region and stiff ones (corresponding to a high-energy barrier) in another region. As an example, in Fig. 4 we show results for such a system set to $d = 17.5$ mm composed of 25 bistable elements with soft connecting elements ($k = 80$ N/m) and 25 bistable elements with stiff connecting elements ($k = 2{,}100$ N/m). As shown in Fig. 3*D*, propagating pulses in these two distinct portions of the system are associated with very

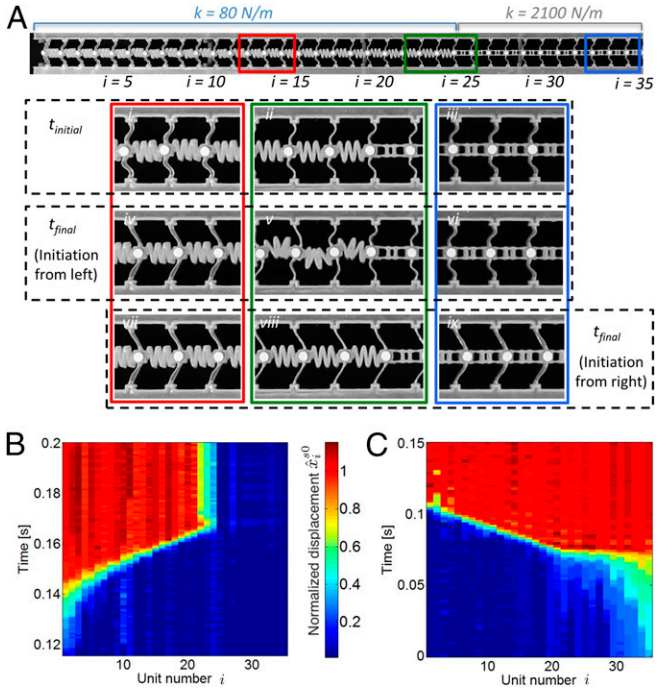


**Fig. 4.** (*A*) A functional soft mechanical diode can be realized by creating a heterogeneous chain composed of a region with soft connectors and a small energy barrier (on the left) and a region with stiff connectors and a large energy barrier (on the right). A pulse initiated in the soft region (from the left) cannot pass into the stiff region due to the large energy barrier, causing the pulse to freeze indefinitely at the interface (*A*, *iv–vi*, and *B*). In contrast (*A*, *vii–ix*, and *C*), when the pulse is initiated in the stiff region, the propagation continues into the soft region and through the whole chain without interruption.

different energy barriers. When a pulse is initiated in the soft region ($k = 80$ N/m), where it possesses a small width (~4 units) and a resulting low-energy barrier ($E_{tot}$ = 0.2–0.3 mJ), it is unable to continue propagating when it reaches the stiff region ($k = 2{,}100$ N/m), where a wide pulse (~20 units) and high-energy barrier are encountered ($E_{tot}$ = 1 mJ). As a result, the pulse freezes indefinitely at the soft–stiff boundary, with the wave energy that has not already been dissipated being stored in the elastic deformation of the local structure (Fig. 4 *A*, *Center*, and *B* and Movie S4). In contrast, a pulse initiated in the stiff region readily propagates through the soft region as well (Fig. 4 *A*, *Bottom*, and *C* and Movie S5), although a kink in wave velocity is observed at the transition between stiff and soft (a result of the change in $k$; Fig. 4*C*). The fact that the wave velocity rapidly changes at the boundary is a manifestation of the system's insensitivity to initial conditions. Also, note that the large-amplitude wave is essentially insensitive to any fabrication-induced imperfections in the system.

As seen above, the final equilibrium wave profile of the system depends on the internal equilibrium between the energy generated by the transition and the energy dissipated by the material damping and is therefore not dependent on the initial conditions. The latter only affect the transient time needed for the pulse to achieve its equilibrium configuration. Indeed, integration of Eq. **3** under the assumption of a smooth, stable propagating wave form shows that the total kinetic energy per mass, $E$, transported by the pulse and its velocity $v$ are related by $E/v = \Delta V/(2\gamma)$ (19), where $\Delta V$ denotes the potential energy difference between the two stable points. The initial conditions (as well as the connector stiffness $k$) do not affect this scaling law.

Using similar principles, more complicated functional devices can be designed, such as mechanical logic gates (Fig. 5). One can define the high-energy state of the bistable element ($x = x^{s0}$ in Fig. 1*D*) as logical state 0 and the low-energy state ($x = x^{s1}$ in Fig. 1*D*) as logical state 1 and then design systems that predictably control pulse propagation in accordance with the energy barrier relationships in Fig. 3*D*. For example, the bifurcated chain in Fig. 5 was designed with a fixed value of $k$ everywhere (80 N/m), corresponding to the left of Fig. 3*D*, with the two input chains set to $d = 17.5$ mm. When the end-to-end distance of the tilted beams in the vertical output chain, $d_{out}$, is small (e.g., $d_{out} = 16.7$ mm), the energy barrier is sufficiently high that both input chains must have been activated by propagating transition waves to continue propagation through the output (Fig. 5*B*), behaving as a soft mechanical logical "and" gate (Movie S6). However, the very same system becomes a logical "or" gate when $d_{out}$ is increased sufficiently (e.g., to $d_{out} = 18.6$ mm), as in Fig. 5*C*. In this case, because the energy barrier of the output chain is smaller (less than 0.1 mJ), if either of the input chains has propagated the transition wave, the wave will propagate through the output chain (Movie S7). Similar behavior can be obtained by other combinations of beam geometries and linear connectors, using Fig. 3*D* as a guide.

## Conclusion

We have designed, printed, and demonstrated a system that enables the propagation of a signal without distortion through soft, dissipative media over arbitrary distances. The soft medium damps out linear waves, leaving only the desired transition wave. The precisely architected system makes use of beam-based units exhibiting asymmetric bistabilities to achieve the propagation of nonlinear transition waves in which the dissipation inherent to the polymer is overcome by the local release of elastically stored energy during the transition of the individual bistable units from a high-energy to a low-energy configuration. The medium thereby undergoes a phase transition as the wave pulse propagates through it. The wave pulse itself locally stimulates the release of the stored elastic energy as it propagates. Although we have used beam pairs as a simple way to produce the (1D) asymmetric bistable potential that we use to store elastic energy along the path of the wave, other higher-dimensional arrangements of beams (5) and shells (31) would also exhibit asymmetric bistability and could therefore also be explored as alternative architectures for the phenomenon studied here.

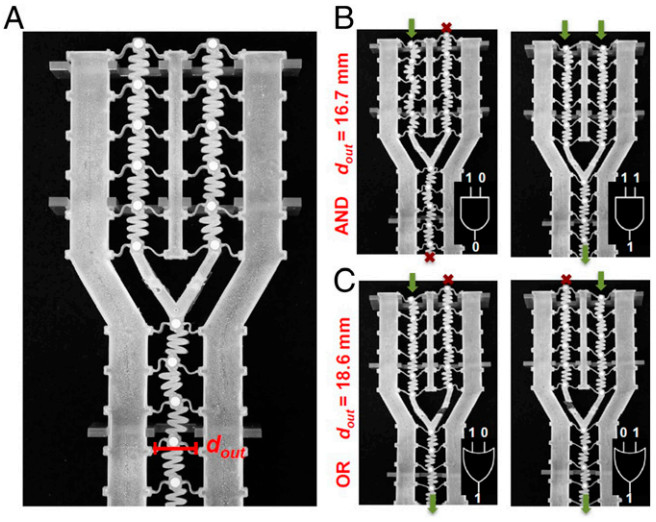


**Fig. 5.** (*A*) A bifurcated chain demonstrating tunable logic in a soft mechanical system. The distance $d_{out}$ determines the logical behavior, producing either an "and" or an "or" gate from the same system. (*B*) When $d_{out}$ is small (in this case, 16.7 mm), the energy barrier is higher, and both input chains must be transitioned in order for the wave to propagate through the output, comprising the function of a logical "and" gate. (*C*) By increasing $d_{out}$ (to 18.6 mm in this case), the energy barrier to continue propagation in the output chain decreases in a predictable manner, producing logical "or" behavior in which a transition wave in either input chain has sufficient energy to initiate propagation in the output chain.

Due to the intrinsically unidirectional transition from the high- to the low-energy state that each individual bistable unit undergoes during propagation, an external source of energy must be provided to reset the bistable elements to their higher-energy state if additional propagation events are desired [which, for example, could be provided pneumatically or via chemical reactions, as has been demonstrated in other soft autonomous systems (37)]. The high quality of the printed elastomer ensures that the system can be reused in this manner indefinitely, with a consistent response from cycle to cycle.

The soft system has the advantage of facile tunability (e.g., changing $d$) and control over wave speed, pulse width, and pulse energy, with pulse propagation independent of the initial conditions. Additionally, the linear coupling springs between the bistable units exert a large effect on pulse width and energy. A simple mechanical model was shown to accurately capture the wave characteristics and guide the design of functional soft logic devices, such as diodes, "or" gates, and "and" gates. This form of logic could be harnessed to introduce some level of feedback and control in truly soft autonomous systems (i.e., without the use of rigid electronics that introduce materials mismatches that can lead to failure). It is also unique in that the system undergoes relatively large-amplitude shape changes during its function, so that the process and output can be easily visualized. As discussed in our previous work (5), the mechanical response of the beams is scale-independent, and the elastic nature of the mechanism ensures a mechanical response that is independent of rate and loading history. Our findings can therefore be adapted to other scales and contexts.

## Materials and Methods

The polydimethylsiloxane (PDMS) structures were produced using direct ink writing, an extrusion-based 3D printing approach (see *Supporting Information* and ref. 5 for more information). The soft architecture was connected to rigid epoxy supports, with the lateral distance between these supports, $d$, controlled by acrylic braces (thereby affecting the morphology of the soft architecture). Copper cylinders were press fit into the printed structure to enable optical tracking of periodic points along the structure. Measurements of the transition waves were made using a high-speed camera (Phantom v7.1), allowing the output of the positions for each element $i$ for all time $[x_i(t)]$. The quasistatic mechanical data were obtained using an Instron 5566 in displacement control.

**ACKNOWLEDGMENTS.** We thank Drs. Sicong Shan, Farhad Javid, and Daniele Foresti for valuable assistance. K.B. and J.A.L. acknowledge support from the Harvard Materials Research Science and Engineering Center (MRSEC) through Grant DMR-1420570. K.B. acknowledges support from the National Science Foundation (NSF) through Grant CMMI-1149456 Faculty Early Career Development (CAREER) Program. N.N. and C.D. acknowledge support from the NSF under Grant CMMI-1200319. D.M.K. acknowledges support from the NSF through CAREER Award CMMI-1254424.

1. Shepherd RF, et al. (2011) Multigait soft robot. *Proc Natl Acad Sci USA* 108(51):20400–20403.
2. Yang D, et al. (2015) Buckling of elastomeric beams enables actuation of soft machines. *Adv Mater* 27(41):6323–6327.
3. Eddington DT, Liu RH, Moore JS, Beebe DJ (2001) An organic self-regulating microfluidic system. *Lab Chip* 1(2):96–99.
4. Carpi F, Frediani G, Turco S, De Rossi D (2011) Bioinspired tunable lens with muscle-like electroactive elastomers. *Adv Funct Mater* 21(21):4152–4158.
5. Shan S, et al. (2015) Multistable architected materials for trapping elastic strain energy. *Adv Mater* 27(29):4296–4301.
6. Restrepo D, Mankame ND, Zavattieri PD (2015) Phase transforming cellular materials. *Extreme Mechanics Letters* 4:52–60.
7. Florijn B, Coulais C, van Hecke M (2014) Programmable mechanical metamaterials. *Phys Rev Lett* 113(17):175503.
8. Nakajima K, Hauser H, Li T, Pfeifer R (2015) Information processing via physical soft body. *Sci Rep* 5:10487.
9. Overvelde JTB, Kloek T, D'haen JJA, Bertoldi K (2015) Amplifying the response of soft actuators by harnessing snap-through instabilities. *Proc Natl Acad Sci USA* 112(35):10863–10868.
10. Marchese AD, Onal CD, Rus D (2014) Autonomous soft robotic fish capable of escape maneuvers using fluidic elastomer actuators. *Soft Robotics* 1(1):75–87.
11. Tolley MT, et al. (2014) A resilient, untethered soft robot. *Soft Robotics* 1(3):213–223.
12. Nesterenko VF (2001) *Dynamics of Heterogeneous Materials* (Springer, New York).
13. Nesterenko VF (1983) Propagation of nonlinear compression pulses in granular media. *J Appl Mech Tech Phys* 24(5):733–743.
14. Spadoni A, Daraio C (2010) Generation and control of sound bullets with a nonlinear acoustic lens. *Proc Natl Acad Sci USA* 107(16):7230–7234.
15. Boechler N, Theocharis G, Daraio C (2011) Bifurcation-based acoustic switching and rectification. *Nat Mater* 10(9):665–668.
16. Fraternali F, Senatore L, Daraio C (2012) Solitary waves on tensegrity lattices. *J Mech Phys Solids* 60(6):1137–1144.
17. Chen BG, Upadhyaya N, Vitelli V (2014) Nonlinear conduction via solitons in a topological mechanical insulator. *Proc Natl Acad Sci USA* 111(36):13004–13009.
18. Nadkarni N, Daraio C, Kochmann DM (2014) Dynamics of periodic mechanical structures containing bistable elastic elements: From elastic to solitary wave propagation. *Phys Rev E Stat Nonlin Soft Matter Phys* 90(2):023204.
19. Nadkarni N, Arrieta AF, Chong C, Kochmann DM, Daraio C (2016) Unidirectional transition waves in bistable lattices. *Phys Rev Lett* 116(24):244501.
20. Liang B, Guo XS, Tu J, Zhang D, Cheng JC (2010) An acoustic rectifier. *Nat Mater* 9(12):989–992.
21. Li F, Anzel P, Yang J, Kevrekidis PG, Daraio C (2014) Granular acoustic switches and logic elements. *Nat Commun* 5:5311.
22. Devaux T, Tournat V, Richoux O, Pagneux V (2015) Asymmetric acoustic propagation of wave packets via the self-demodulation effect. *Phys Rev Lett* 115(23):234301.
23. Lewis JA (2006) Direct ink writing of 3D functional materials. *Adv Funct Mater* 16(17):2193–2204.
24. Smay JE, Cesarano J, III, Lewis JA (2002) Colloidal inks for directed assembly of 3-D periodic structures. *Langmuir* 18(14):5429–5437.
25. Gratson GM, Xu M, Lewis JA (2004) Microperiodic structures: Direct writing of three-dimensional webs. *Nature* 428(6981):386.
26. Ahn BY, et al. (2009) Omnidirectional printing of flexible, stretchable, and spanning silver microelectrodes. *Science* 323(5921):1590–1593.
27. Forterre Y, Skotheim JM, Dumais J, Mahadevan L (2005) How the Venus flytrap snaps. *Nature* 433(7024):421–425.
28. Timoshenko SP (1935) Buckling of flat curved bars and slightly curved plates. *J Appl Mech* 2(1):17–20.
29. Fargette A, Neukirch S, Antkowiak A (2014) Elastocapillary snapping: Capillarity induces snap-through instabilities in small elastic beams. *Phys Rev Lett* 112(13):137802.
30. Pandey A, Moulton DE, Vella D, Holmes DP (2014) Dynamics of snapping beams and jumping poppers. *Europhys Lett* 105(2):24001.
31. Bende NP, et al. (2015) Geometrically controlled snapping transitions in shells with curved creases. *Proc Natl Acad Sci USA* 112(36):11175–11180.
32. Fraternali F, Carpentieri G, Amendola A, Skelton RE, Nesterenko VF (2014) Multiscale tunability of solitary wave dynamics in tensegrity metamaterials. *Appl Phys Lett* 105(20):201903.
33. Khatri D, Ngo D, Daraio C (2012) Highly nonlinear solitary waves in chains of cylindrical particles. *Granul Matter* 14(1):63–69.
34. Molerón M, Leonard A, Daraio C (2014) Solitary waves in a chain of repelling magnets. *J Appl Phys* 115(18):184901.
35. Nadkarni N, Daraio C, Abeyaratne R, Kochmann DM (2016) Universal kinetic energy transport law for dissipative and diffusive phase transitions. *Phys Rev B* 93(10):104109.
36. Le T-N, Battini J-M, Hjiaj M (2011) Efficient formulation for dynamics of corotational 2D beams. *Comput Mech* 48(2):153–161.
37. Wehner M, et al. (2014) Pneumatic energy sources for autonomous and wearable soft robotics. *Soft Robotics* 1(4):263–274.

# Supporting Information

Raney et al. 10.1073/pnas.1604838113

## Experiments

**Fabrication.** The structures were produced using direct ink writing, an extrusion-based 3D printing method, followed by an infilling step. A viscoelastic polydimethylsiloxane (PDMS) ink was used for 3D printing. This consisted of a shear-thinning PDMS material, Dow Corning SE-1700 (85 wt %), with a lower-viscosity PDMS additive, Dow Corning Sylgard 184 (15 wt %). The viscoelastic yield properties are tailored (see supporting information in ref. 5 for rheological characterization) to ensure that the uncured ink both flows readily during printing, yet maintains its shape until it is permanently cross-linked in a subsequent curing step (100° C for 30 min). This material was extruded through a tapered nozzle (200 μm inner diameter tapered nozzle from Nordson EFD) during programmed translation of the nozzle over a fixed substrate (PTFE-coated aluminum). Ink extrusion was controlled via fixed pressure (Nordson EFD Ultimus V pressure box), with the nozzle precisely positioned using a custom 3D positioning stage (Aerotech). After printing and curing of the PDMS ink, two regions parallel with and adjacent to the functional region of wave propagation were infilled with epoxy (Momentive Epon 828) to prevent undesired structural bending that would make measuring the response of the system difficult. The lateral distance between these rigid supports, $d$, is defined by acrylic braces of precise dimensions, which were made using an Epilog Laser Mini cutting system. The acrylic braces also serve to elevate the soft structure (via the epoxy supports) without contacting it, to eliminate any interactions between the wave pulse and the table surface. A cylindrical copper rod (3.175 mm diameter) was cut to pieces of 5.17 mm length (giving a mass of ∼0.47 g), which were press fit into the printed structure to enable optical tracking of periodic points along the structure. The top surfaces of these copper cylinders were painted with flat white paint to produce excellent light contrast for visualization of the transition wave propagation.

To achieve a range of effective stiffnesses $k$, several different geometries were designed for the linear coupling elements that connect the individual bistable elements to one another. As shown in Fig. S1, we measured stiffness values ranging from 30 to 2,100 N/m (as measured with a commercial quasistatic test system, Instron 5566, in displacement control at a displacement rate of 2 mm/min). Additional intermediate values can be obtained by varying the translation speed of the printhead during the printing process.

**Small-Amplitude Excitation.** To characterize the dynamic response of the system, we considered small-amplitude excitations with white noise up to 5 kHz generated by an electrodynamic shaker (model K2025E013; Modal Shop) directly connected to one end of the sample. We monitored the propagation of the mechanical signal using two miniature accelerometers (352C22; PCB Piezotronics) attached to both ends of the chain (Fig. S2*A*). Spectra were obtained for three different chain lengths (6, 15, and 50 bistable units in length) and were determined to be independent of $d$. The rigid epoxy supports were held apart at fixed distances by acrylic braces. These ensured that the morphology of the soft structure remained in a controlled configuration during the dynamic tests. The acrylic braces were in turn glued to steel laboratory stands on an optics table, to minimize undesired vibrations. As expected for a soft, dissipative material, the transmittance spectra [defined as the ratio between the measured output and input accelerations, $A_{\text{out}}(\omega)/A_{\text{in}}(\omega)$] clearly indicate that small-amplitude excitations are rapidly dissipated due to the strong damping intrinsic to the material (Fig. S2*B*). In fact, at frequencies above 550 Hz, all energy is essentially dissipated before traveling through only six bistable units (independently of the direction of transmission or the state of the bistable elements). For longer distances (50–100 repeating units), even lower frequencies (100 Hz or less) show a drop of at least 20 dB through the structure, meaning that no more than about 1% of the input acceleration is measured at the output for these low frequencies. These results confirm that the material from which the medium is architected is intrinsically highly dissipative and does not enable propagation of small-amplitude elastic waves over long distances.

**Measuring Transition Waves.** Measurements of the transition waves were made using a high-speed camera (Phantom v7.1). For systems with low wave speeds (usually $k = 80$ N/m and $v$ on the order of a few meters per second), a 500-Hz recording rate was used. For higher-speed systems (usually $k = 2{,}100$ N/m and $v$ between 10 and 20 m/s) a higher recording rate of 1,000 Hz was used. Two halogen floodlights were positioned to provide sufficient lighting for the high-speed camera to record the experiments solely with light reflected from the sample. After recording the wave experiment with the high-speed camera, custom code in MATLAB was used to track the locations of each bistable element, allowing the output of the positions for each element $i$ for all time, $x_i(t)$.

**Control of Wave Propagation.** Although the results reported in Fig. 3 were obtained numerically, we also experimentally characterized the propagation of large-amplitude waves in systems characterized by different values of $k$ and $d$.

First, to validate the numerical predictions for the on-site potential, we performed quasistatic 1D displacement-controlled experiments for different $d$ values on an individual bistable element. The experimental results reported in Fig. S5 show a convincing agreement with the numerical results (Fig. 3*A*).

Next, we experimentally investigated the effect of $d$ and $k$ on both wave velocity and pulse width.

To explore the effect of $d$ on the wave behavior, we tested the propagation of a transition wave through a system in which different values of $d$ were assigned for the different experiments (Fig. S6). This can be done without fabricating a new sample for each experiment because different values of $d$ can be achieved by applying a defined lateral displacement ($d = 17.5$ and 18.6 mm in Fig. S6). Comparison between the experimental results shows an evident change in slope of the interface between the pretransitioned and posttransitioned states (blue and red, respectively), indicating a variation in pulse velocity (the slope of the interface is inversely proportional to the speed). In particular, we observe a change in the wave speed from about 1.9 to 3.4 m/s for $d = 17.5$ mm and $d = 18.6$ mm, respectively, in a system for which $k = 80$ N/m. In contrast, it is apparent that the pulse width is not significantly affected by $d$, as the number of bistable elements in the midst of transitioning between solid blue and solid red remains approximately constant as a function of time.

The stiffness of the linear connecting elements, $k$, also greatly affects the pulse propagation. Fig. S8 *A* and *B* show data for an experiment conducted on a system with stiff and soft connecting elements (2,100 N/m and $k = 80$ N/m, respectively; Fig. S8*C*, *Insets*). First, by comparing the slope of the boundaries in Fig. S8 *A* and *B*, it is evident that the stiffness of the connecting elements affects the pulse velocity. In fact, we find velocities of ∼18 and 3.4 m/s for $k = 2{,}100$ N/m and $k = 80$ N/m, respectively. Moreover, $k$ strongly affects the pulse width (i.e., the number of bistable elements that at any given time are simultaneously in the process of transitioning between stable states). This is evident in Fig. S8*C*,

where we compare experimental snapshots of $\hat{S}_i$ for the two systems and observe widths of ~25 and 4 elements for $k = 2{,}100$ N/m and $k = 80$ N/m, respectively.

## Simulations

**Computation of the On-Site Potential.** One bistable beam element consists of two inclined beams with a mass placed at the center. Because the mass is rigid compared with the compliant beams, it is assumed that the force on the mass by the bistable structure is produced solely by the deformation of the beams. Due to the symmetry of the structure, the quasistatic deformation of only one tilted beam was modeled with appropriate boundary conditions. The beam was modeled using slender corotational beam finite elements (36) whose one-dimensional stretching and bending deformation are governed by a nonlinear Neo-Hookean material model with an initial slope of $E = 1.8$ MPa. Results of an example simulation are shown in Fig. S3*A*. The undeformed beam is first subjected to an initial vertical precompression $v_0$ according to the $d$ value. The boundary node B is then displaced horizontally from one stable point to another in displacement control and the resulting force required is recorded. The force–displacement function obtained in this way is fit with a seventh-order polynomial. The force–displacement polynomial is validated by comparison with the experimentally measured force–displacement curve for $d = 17.5$ mm, as shown in Fig. S5*B*; note that the computed forces are multiplied by 2 to account for the force of one bistable element containing two tilted beams. This simulation was repeated for different $d$ values to compute $V(x, d)$.

**Parameters.** The mass at each node was 0.419 g, with $k$ ranging from 50 to 2,500 N/m and $d$ ranging from 14.5 to 19.0 mm with $d = 19.0$ mm corresponding to the undeformed state, and the dissipation parameter of 0.08 N.s/m optimized by matching the computational and experimental velocity at $(k, d) = (80$ N/m, 17.5 mm) (see Fig. S4 for the comparison of experimental and simulation results by which the dissipation parameter was determined).

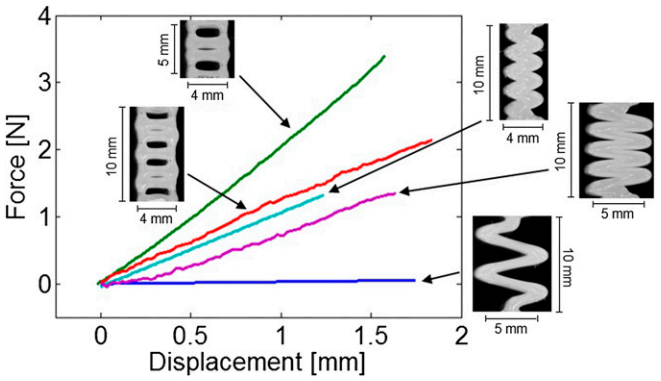


**Fig. S1.** Using different geometries for the linear coupling elements leads to different effective spring stiffnesses, which greatly affect the width and velocity of the propagating pulse. The stiffnesses were measured using an Instron 5566 in displacement control with a rate of 2 mm/min. The measured stiffnesses of the linear elements shown here were measured to vary from 30 to 2,100 N/m.

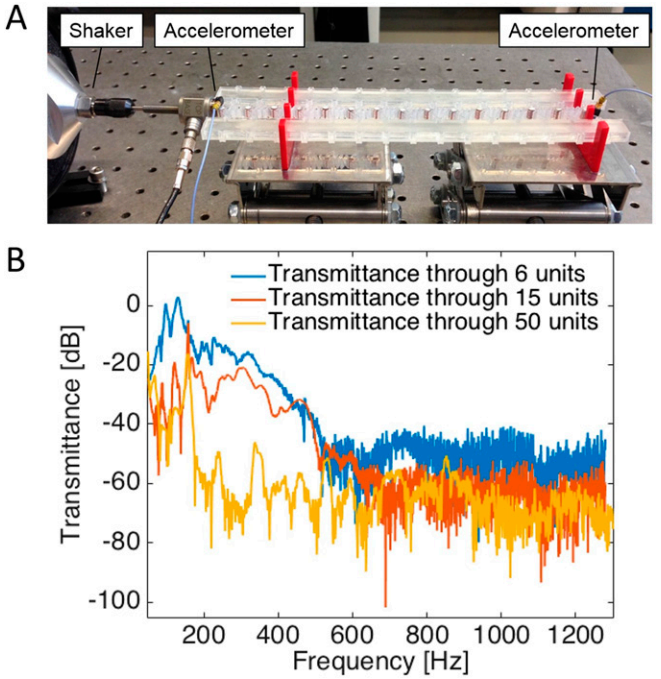


**Fig. S2.** (*A*) The shaker (on the left) was attached to an accelerometer that was directly glued to the samples. The accelerator used to measure the output was glued to the other end of the sample. The acrylic braces (red) were used to hold the soft architecture at well-defined widths and were glued to the laboratory stands to prevent unwanted movement. (*B*) Small-amplitude, linear excitation from either end of the chain is rapidly dissipated due to the damping intrinsic to the polymer, as is particularly evident with increasing frequency, shown here for samples with 6, 15, and 50 bistable units.

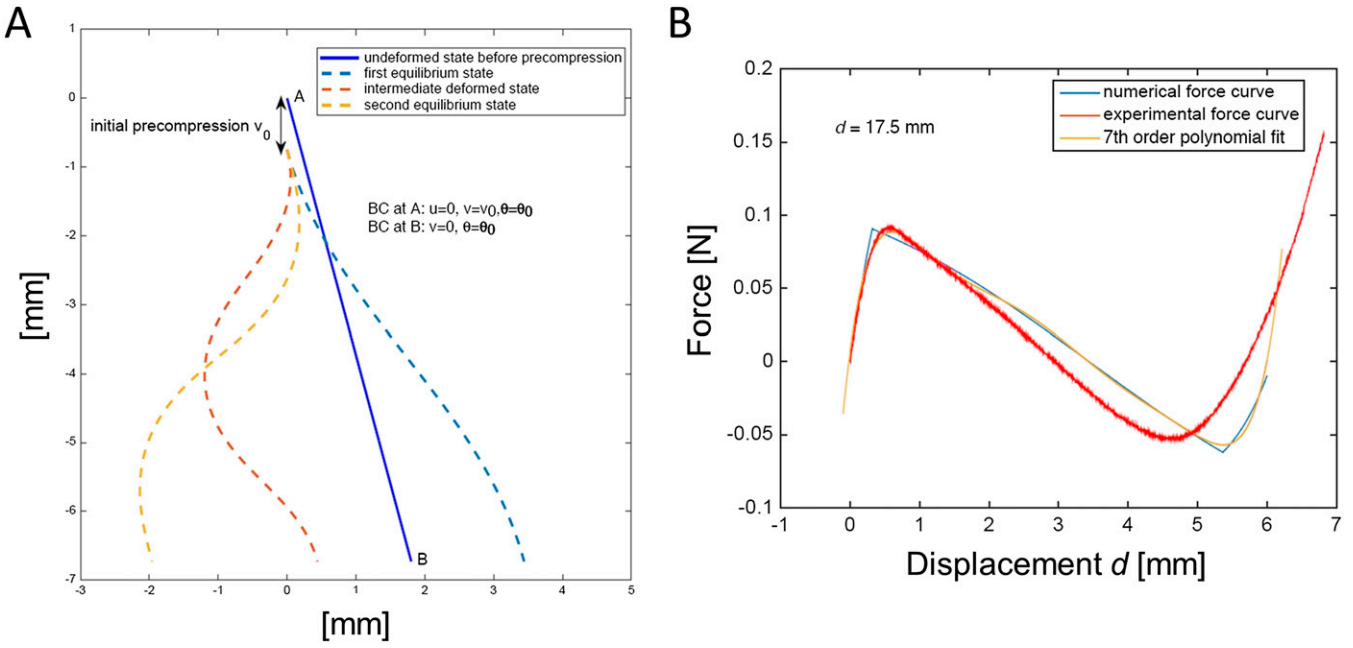


**Fig. S3.** (*A*) An example of the beam deformation simulation is shown. All simulations were performed on only one half of the bistable element (i.e., on one tilted beam). Different configurations of the beam are shown as it is displaced from one stable configuration to another. The force at node B is measured (and doubled to account for bistable element consisting of two tilted beams). (*B*) The numerical, experimental, and best-fit force–displacement curves are shown for $d = 17.5$ mm. The graphics indicate that experimental and numerical results are in good agreement.

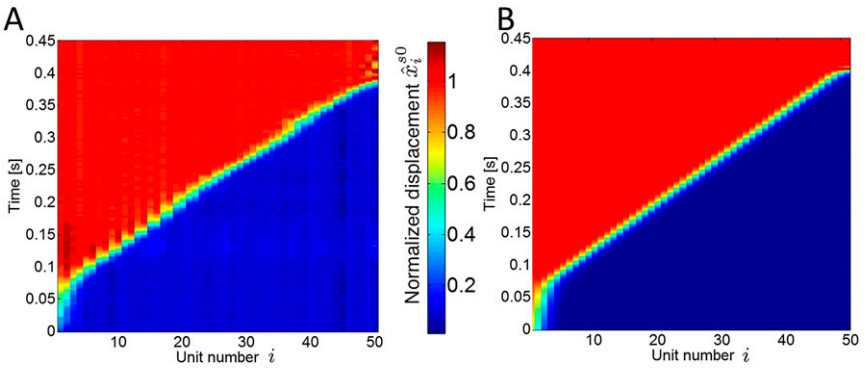


**Fig. S4.** (*A*) Experimental and (*B*) simulation results corresponding to $(k, d)$ = (80 N/m, 17.5 mm), as used to determine the dissipation parameter in the model.

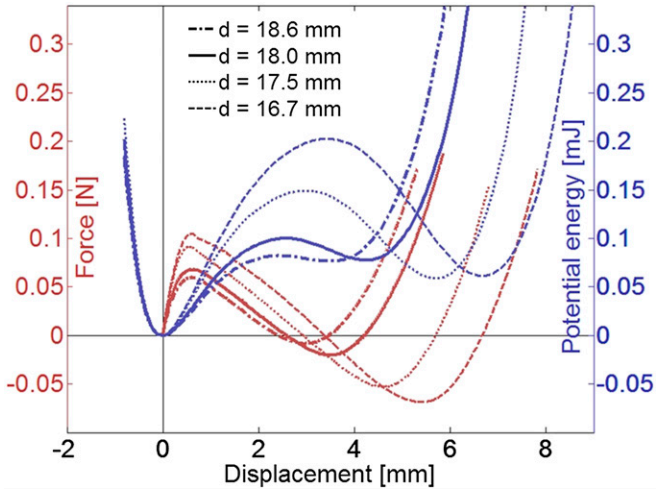


**Fig. S5.** Experimental data obtained by directly measuring the force–displacement behavior of a single bistable element for different lateral constraints, *d*. The potential energy is calculated from this, showing a large effect of *d* on the energy barrier of the bistable elements.

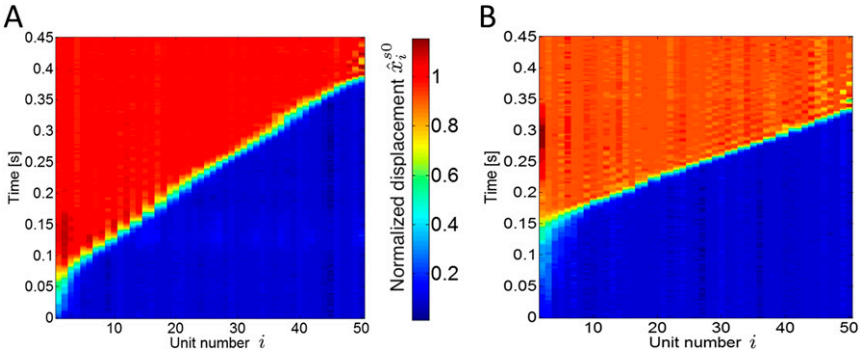


**Fig. S6.** (*A*) Experiments show that when *d* is small (17.5 mm here), the energy barrier between the two stable states is larger, and the wave propagation is slower. (*B*) When *d* is larger (18.6 mm here), the smaller energy barrier allows a larger propagation speed, as evidenced by the changed slope.

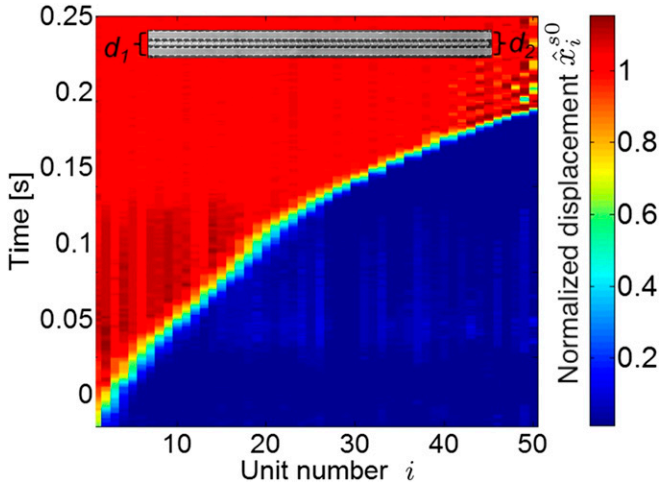


**Fig. S7.** Because the system is deformable, different values of *d* can be used along the length of the system, resulting in spatially varying energy barriers to propagation; this can be used to vary the velocity along the length of the chain, as it is here for a gradient structure (*d* is about $d_1 = 14.5$ mm at the left end and about $d_2 = 19.0$ mm at the right end, corresponding to measured speeds of 0.8 and 5.2 m/s, respectively).

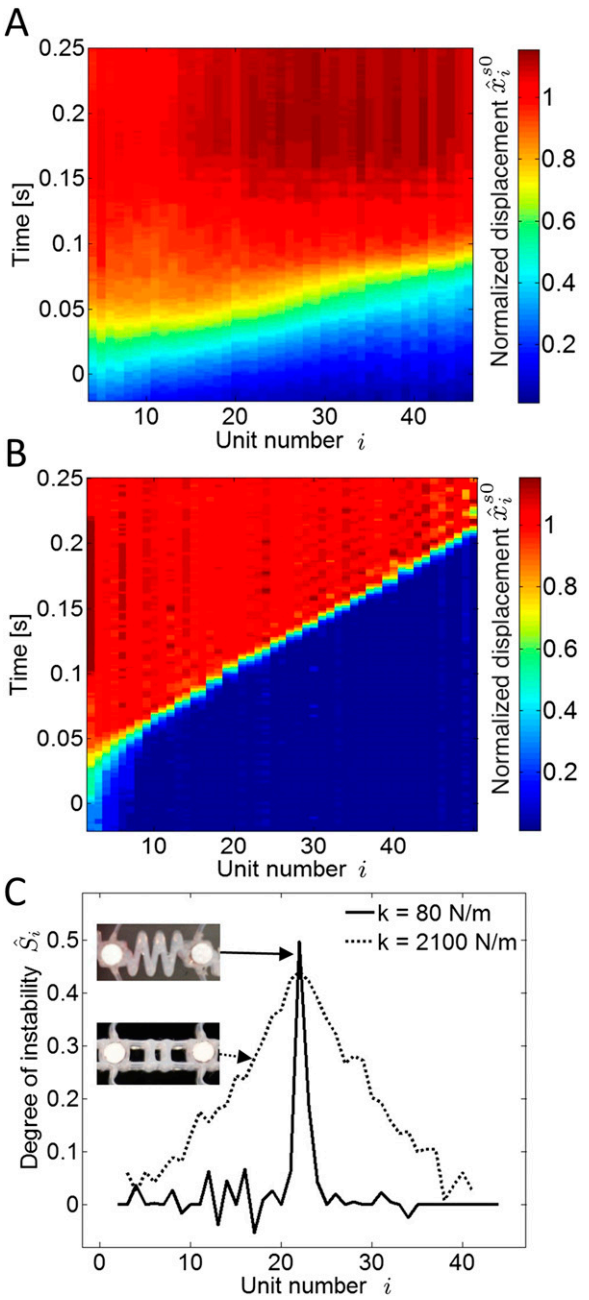


**Fig. S8.** (*A*) When *k* is high (2,100 N/m here), experiments show that both the pulse width and the pulse velocity (as determined by the slope) are much higher, even with the same value of *d* (18.6 mm), than (*B*) when *k* is low (80 N/m here). (*C*) The same comparison can be made by taking experimental snapshots of the two different systems ($k$ = 80 N/m and $k$ = 2,100 N/m, corresponding to the differences in morphology of these elements, as pictured in *Insets*).

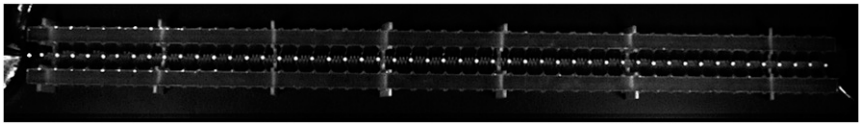

**Movie S1.** An example raw movie of a propagation event ($d = 18.6$ mm, $k = 80$ $N/m$) as filmed via a high-speed camera (Phantom v7.1) at 500 Hz and replayed at 25 Hz.

Movie S1

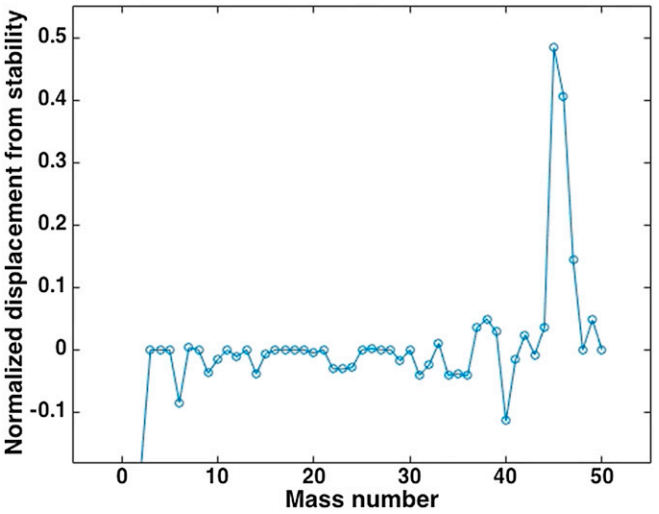


**Movie S2.** The propagation event from Movie S1, with the locations of the individual bistable elements tracked. The quantity being plotted is $\hat{S}_i$, the minimum normalized distance to the nearest stable configuration for each of the $i$ bistable elements.

Movie S2

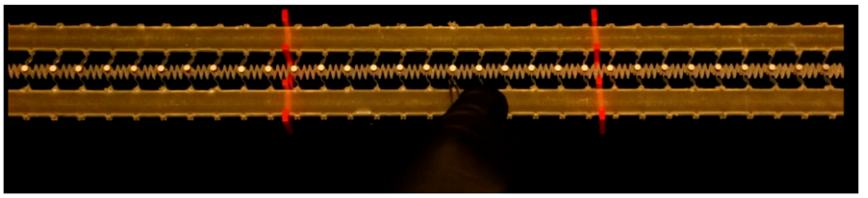

**Movie S3.** A propagation event recorded in real time for which propagation is initiated in the center of the system, resulting in the propagation of a tensile pulse in one direction and a compressive pulse in the other direction (with equal speed and pulse width).

Movie S3

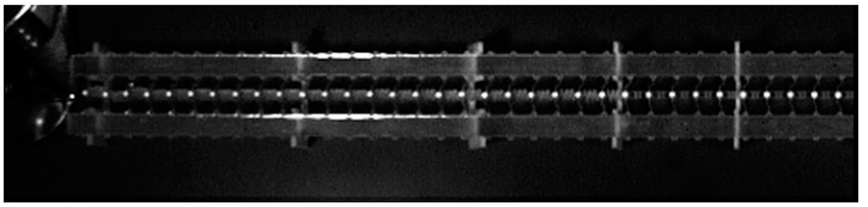

**Movie S4.** High-speed camera movie of diode behavior in a heterogeneous system ($k = 80$ N/m on the left and $k = 2{,}100$ N/m on the right of the system). The pulse is initiated in the soft region on the left and does not have sufficient energy to propagate into the stiff region on the right.

Movie S4

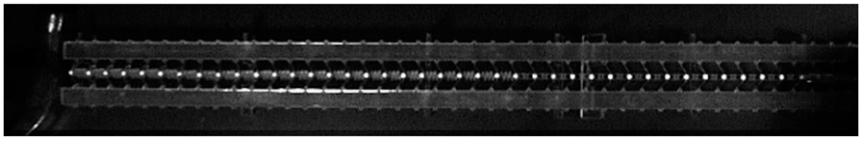

**Movie S5.** The same heterogeneous system of Movie S4 but now with a pulse initiated in the stiff region on the right. The pulse has sufficient energy to pass through the interface and through the soft region on the left.

Movie S5

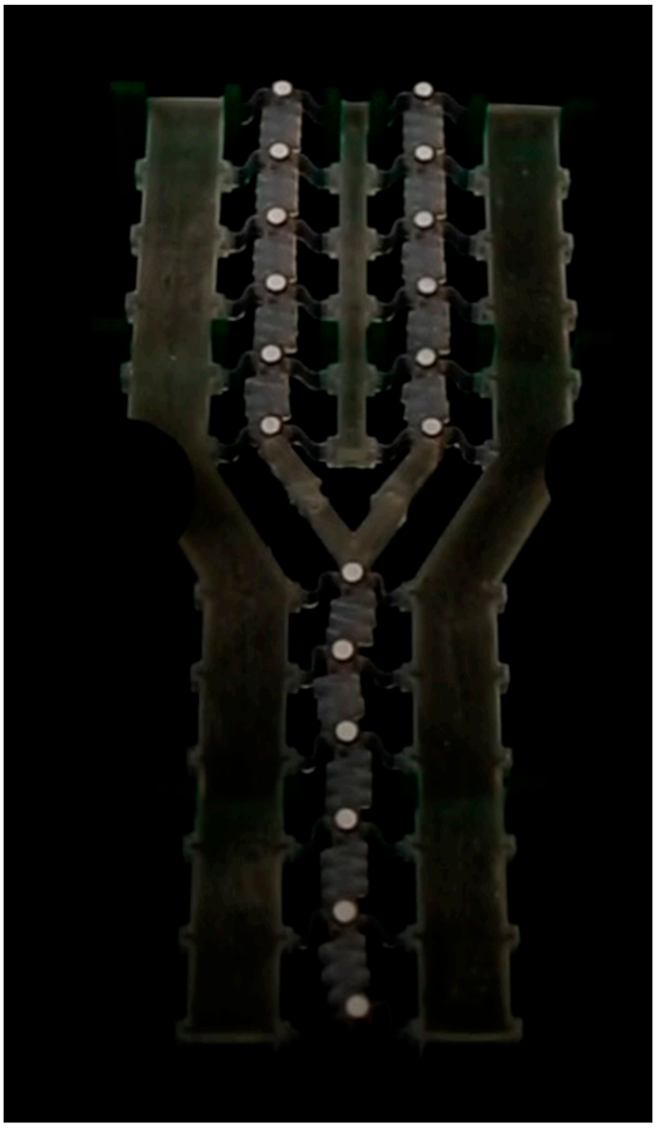

**Movie S6.** A bifurcated system in which functional "and" behavior is realized through the control of the spacing in the output chain ($d_{out} = 16.7$ mm). Both input chains must be activated in order for a pulse to propagate in the output chain.

Movie S6

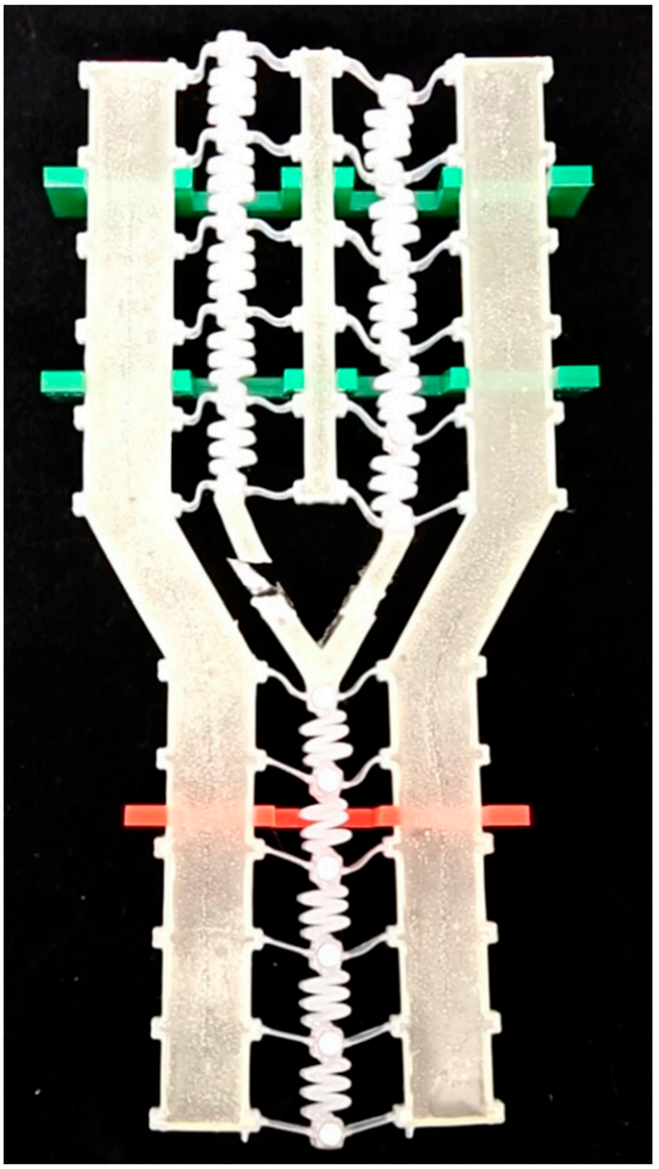

**Movie S7.** The same bifurcated system as in Movie S6 but now with $d_{out}$ increased to 18.6 mm. Because of the concomitant decrease in the energy barrier, the activation of either input chain is sufficient to continue wave propagation through the output chain (functional "or" behavior).

Movie S7